**AALBORG UNIVERSITY**

# State-of-Charge Balance Using Adaptive Droop Control for Distributed Energy Storage Systems in DC MicroGrid Applications

Lu, Xiaonan; Sun, Kai; Guerrero, Josep M.; Vasquez, Juan Carlos; Huang, Lipei

# State-of-Charge Balance Using Adaptive Droop Control for Distributed Energy Storage Systems in DC Micro-Grid Applications

Xiaonan Lu, *Student Member*, *IEEE*, Kai Sun, *Member*, *IEEE*, Josep M. Guerrero, *Senior Member*, *IEEE*, Juan C. Vasquez, *Member*, *IEEE*, Lipei Huang

*Abstract* - **This paper presents the coordinated control of distributed energy storage systems (DESSs) in DC micro-grids. In order to balance the state-of-charge (SoC) of each energy storage unit (ESU), an SoC-based adaptive droop control method is proposed. In this decentralized control method, the droop coefficient is inversely proportional to the $n^{th}$ order of SoC. By using SoC-based droop method, the ESUs with higher SoC deliver more power, while the ones with lower SoC deliver less power. Therefore, the energy stored in the ESU with higher SoC decreases faster than that with lower SoC. The SoC difference between each ESU gradually becomes smaller and finally the load power is equally shared between the distributed ESUs. Meanwhile, the load sharing speed can be adjusted by changing the exponent of SoC in the adaptive droop control. The model of SoC-based adaptive droop control system is established and the system stability is thereby analyzed by using this model. Simulation and experimental results from a 2×2.2 kW parallel converter system are presented in order to validate the proposed approach.**

*Index Terms*—**Droop control; distributed energy storage system (DESS); DC micro-grids; state-of-charge (SoC)**

## I. Introduction

With the objective to electrify remote areas and energy islands, the micro-grid concept is gaining more and more popularity [1]. Nowadays DC micro-grids are becoming more attractive with the raise of DC power sources, storages, and the loads with natural DC coupling, e.g. photovoltaic modules, batteries, fuel cells, LEDs, and so on. With the comparison of the overall efficiency, it can be found that the efficiency of DC system is higher than the AC system [2]-[3]. At the same time, DC do not require for

synchronization, and the problems caused by the reactive power and harmonics disappear. For these reasons, recently there is an increasing awareness on DC micro-grids [4]-[11]. A typical configuration of DC micro-grid is shown in Fig. 1 [10].

The control of the power electronics converters in the distributed generation has been intensively studied in the past years. Among them, the droop control and its variants are commonly accepted as the methods to integrate several voltage sources in a micro-grid [5]-[6], [9]-[12]. Basically, by using a control loop, it reduces linearly the output voltage reference when the output power increases. The output power of the power electronics interface converter should be inversely proportional to the droop coefficient.

In order to solve the uncertainty problem of the renewable energy sources, distributed energy storage units (ESUs) are commonly adopted in a micro-grid [12]. The control scheme of an energy storage system (ESS) commonly consists of two parts: one of them is the battery management system (BMS) and the other one is the power converter system (PCS). The configuration of the above two control systems in a microgrid with distributed ESUs is shown in Fig. 2.

The function of the BMS is to balance the SoC and output voltage of each cell in the battery string. Several literatures focus on the BMS. In [13], a modular charge equalizer for Lithium battery strings is proposed, where the modularization is applied to a string of four cells and the system is composed of one module balancing circuit and two intra-module equalizers. In [14], a method based on redundancy cells is presented, where the system is controlled to dynamically disconnect a redundant cell from the battery pack in order to reach an optimal balancing result. In [15], a screening process is involved to improve the performance of output voltage and SoC balancing.

Although the BMS is useful for balancing the SoC of each cell in a battery string, it is not enough for the applications of distributed generation systems, like microgrids. Each BMS can be used for only one ESU, while is not capable of the SoC balancing between different ESUs. For example, as shown in Fig. 2, ESU #1 is composed of a battery string and the BMS is employed locally to balance the SoC of each cell in this string. However, the BMS cannot be used to balance the overall SoCs between ESU #1

and ESU #2. The SoC balancing between different ESUs should be accomplished by the PCS.

Aiming at the PCS, in [16]-[17], the configuration of cascade H-bridges is employed to balance the SoC of each ESU. In [18], a low-pass filter in the control diagram is employed to improve the load distribution of an ESS which consists of composite kinds of ESUs. However, the above methods are all achieved by centralized controllers, which are not suitable for decentralized configuration of a microgrid. In [11], a fuzzy control system is employed to adjust the output power of each ESU. Although the method is implemented based on droop control, the calculation of the average stored energy is still necessary. As a result, the method is also communication–dependent since the stored energy of each ESU is transferred to the others to calculate the average value.

The optimal SoC balancing in a microgrid with ESUs should consist of two aspects: 1) the SoC of each cell in one ESU is balanced by the BMS; 2) the overall SoC of each ESU is equalized by the PCS. Since in the existing literatures there are kinds of valid methods developed for the first requirement, the BMS is not the research subject here. In this study, an SoC balancing method for different distributed ESUs are proposed, which is employed to meet the second requirement and implemented in the PCS. Meanwhile, the proposed method is achieved based on droop control and accomplished locally without any communications between different interfacing converters. At the same time, in this method, the droop coefficient is adaptively adjusted according to the SoC. In particular, it is set inverse-proportionally to the $SoC^n$. By changing the value of the exponent n, the SoC balancing and output power equalization speed can be regulated. A flexible operation of a DC microgrid with distributed ESUs can be achieved. Furthermore, it should be pointed out that this work focuses on the DESS with similar kinds of ESUs. If the power ratings and capacities of the ESUs differ significantly, the variable state-of-power (SoP) can be used instead of SoC, in order to reach the proper power sharing. The SoP balancing can be achieved in this condition.
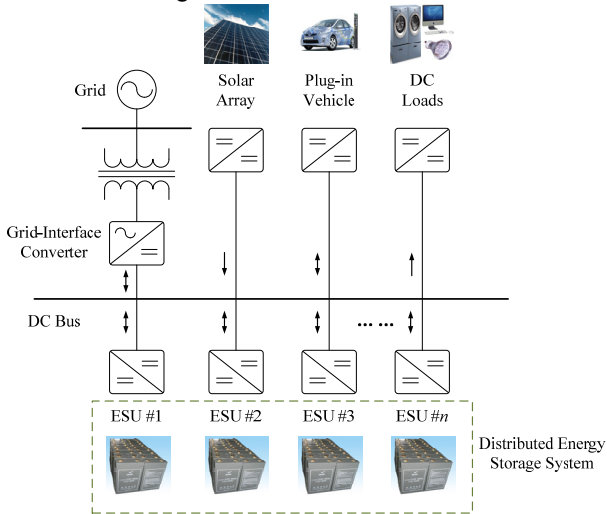


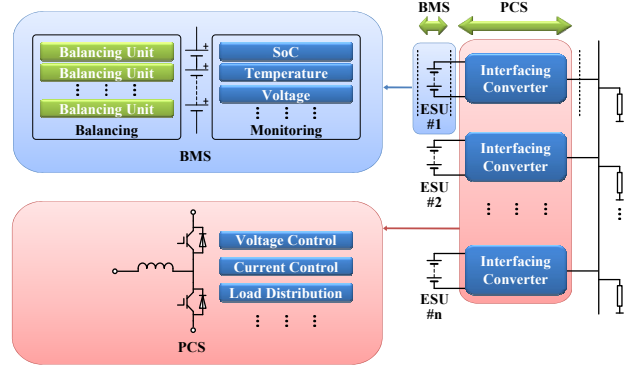Fig. 1. Typical configuration of a DC micro-grid.



Fig. 2. Configuration of BMS and PCS in a microgrid with distributed ESUs.

Meanwhile, although the proposed method is validated by using the laboratory scale test, it is not just suitable for the system with low power rating. Since it is developed based on commonly used droop control, it can be used in the distribution systems with different power ratings. If the method is employed in a high power distribution system, only an ESU with suitable rating is required and the approach for balancing the SoC and the output power are not necessary to change.

## II. PROPOSED SOC-BASED DROOP CONTROL METHOD

### A. Basic Operation Modes of the DESS

In order to clearly describe the usage of the proposed control method, the basic operation modes of the DESS is shown as follows.

When the sufficient amount of input power is provided in the microgrid, the load is fed by the renewable energy sources and meanwhile the ESUs operate in the charging mode. In the charging process, in order to rapidly reach the fully charged state, the ESUs are charged with maximum input power. When the ESU is fully charged, it is disconnected and waits for the discharging process.

When the input power of the renewable energy sources are not enough for feeding the load in the microgrid, the ESUs turn to discharging mode. In the discharging process, the optimal condition is that the SoC of each ESU is balanced and the output power of each ESU is equalized. Here, the proposed SoC-balancing method based on droop control is employed. With this control method, the load power is shared according to the SoCs. Meanwhile, the SoC in each ESU is balanced.

### B. Model of the ESU

As aforementioned in Section I, the research subject of this paper is focused on PCS and the proposed method is achieved by using droop control. The function of the ESU model is only to show the key parameters, like SoC, for the usage of the following PCS stage. Hence, a brief ESU model is used here with the configuration of a voltage source representing the open circuit voltage $v_{oc}$ and an internal output resistance $Z_{eq}$ for each cell, as shown in Fig. 3. Meanwhile, the basic coulomb counting method is

employed to estimate the SoC, as shown in (1).

$$SoC_i = SoC_{i\,t=0} - \frac{1}{C_e}\int i_{in\_i}dt \qquad (1)$$

where $SoC_{i\,t=0}$ is the initial value of SoC, $C_e$ is the capacity of the ESU, $i_{in\_i}$ is the input current of the interfacing converter (the output current of the ESU), and i = 1, 2.

Both $v_{oc}$ and $Z_{eq}$ can be calculated by the function of $SoC$ and $T$, where $T$ is the ambient temperature. It can be demonstrated that the $v_{oc}$ highly depends on $SoC$, while it does not change significantly with the variation of $T$ [19]. Meanwhile, the ambient temperature has a major influence on $Z_{eq}$, which almost does not change with $SoC$ [20]. As a result, $v_{oc}$ and $Z_{eq}$ can be reached as

$$v_{oc} = f_1(SoC) \qquad (2a)$$

$$Z_{eq} = f_2(T) \qquad (2b)$$

where $T$ is the ambient temperature.

Functions $f_1$ and $f_2$ can be achieved by data fitting. The results are shown below:

$$v_{oc} = a_{v1}\cdot e^{a_{v2}\cdot SoC} - a_{v3}\cdot e^{-a_{v4}\cdot SoC} \qquad (3a)$$

$$Z_{eq} = a_{z1}\cdot T^2 - a_{z2}\cdot T + a_{z3} \qquad (3b)$$

where the coefficients are shown in Table I.

### C. Model of the SoC-based Droop Control System

Considering a voltage-controlled power electronics converter, the conventional droop control method can be expressed as

$$v_{dc} = v_{dc}^* - m_p\cdot p_{lpf} \qquad (4)$$

where $v_{dc}$ and $v_{dc}^*$ are the DC output voltage and its reference values, $p_{lpf}$ is the filtered output power by the low-pass filter, and $m_p$ is the droop coefficient.

When the input sides of the parallel converters are connected to the distributed ESUs, it is necessary to share the power according to the SoC of each unit. It is commonly known that the droop coefficient should be inversely proportional to the output power. Thus, if the droop coefficient is selected to be inversely proportional to the $SoC^n$, the output power of each converter will be proportional to each $SoC^n$. In other words, the ESUs with higher SoC deliver more power, while the ones with lower SoC deliver less. In a parallel converter system with two modules, the droop control method can be rewritten as

$$v_{dc\,i} = v_{dc}^* - (m_0 / SoC_i^n)\cdot p_{lpf\_i} \qquad (5)$$

where $m_0$ is the initial droop coefficient for fully charged condition, n is the exponent of SoC, and i = 1, 2.
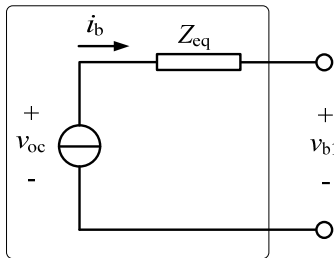


Fig. 3. Model of each cell.

| $v_{oc}$ /V | | | |
|---|---|---|---|
| $a_{v1}$ /V | $a_{v2}$ /- | $a_{v3}$ /V | $a_{v4}$ /- |
| 3.228 | $3.934\times10^{-4}$ | $7.681\times10^{-1}$ | $2.294\times10^{-1}$ |

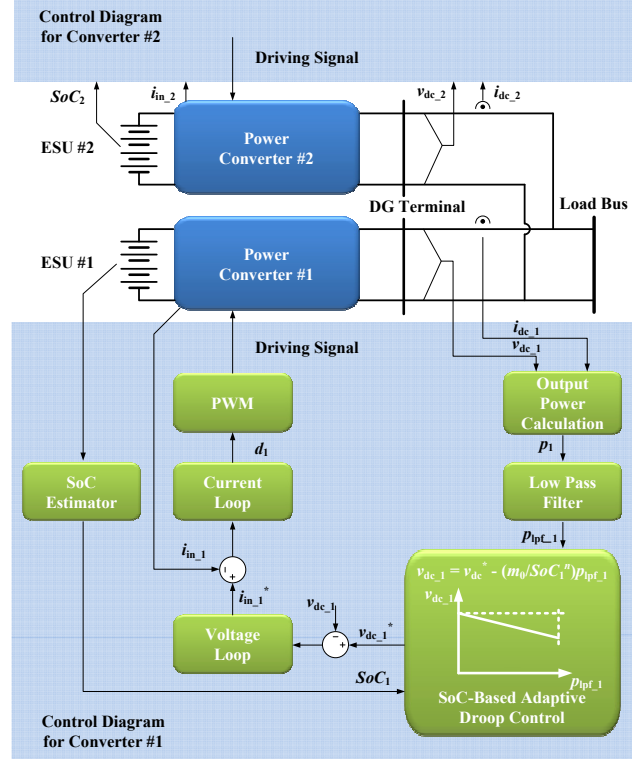| $Z_{eq}$ /$\Omega$ | | |
|---|---|---|
| $a_{z1}$ /$\Omega$°C$^{-2}$ | $a_{z2}$ /$\Omega$°C$^{-1}$ | $a_{z3}$ /$\Omega$ |
| $4.405\times10^{-7}$ | $4.087\times10^{-5}$ | $1.701\times10^{-3}$ |



Fig. 4. Control diagram of the SoC-based adaptive droop control system.

Here, the exponent n is involved to adjust the SoC-balancing speed, which will be demonstrated and evaluated in the following subsection. The control diagram of the whole system is shown in Fig. 4. Since the control diagrams for Converter #1 and #2 are the same, the latter one is not shown here for brevity.

By perturbing (5) and transferring the results into s domain, the following model can be obtained for both converters:

$$m_0\cdot \hat{p}_{lpf\_i} = nSoC_i^{n-1}(V_{dc}^* - V_{dc\_i})\cdot \hat{SoC}_i - SoC_i^n\cdot \hat{v}_{dc\_i} \qquad (6)$$

where $\wedge$ denotes the perturbed values, $SoC_i$, $V_{dc\_i}$ and $V_{dc}^*$ show the equilibrium point values, and i = 1, 2.

Meanwhile, neglecting the power losses in the interface converter, it yields that:

$$p_i \approx p_{in\_i} = v_{in\_i}i_{in\_i} \qquad (7)$$

where $p_i$ is the output power without filtering, $p_{in\_i}$ is the input power of the interfacing converter (output power of the ESU), $v_{in\_i}$ and $i_{in\_i}$ are the input voltage and current of the interfacing converter (output voltage and current of the ESU), and i = 1, 2.

Considering that SoC varies very slowly, and the output voltage of each ESU almost maintains constant in a large range of SoC, it can be assumed that the output voltage of

each unit keeps constant. Therefore,

$$v_{\text{in\_i}} = V_{\text{in\_i}} \tag{8}$$

where $V_{\text{in\_i}}$ is the constant DC output value, and i = 1, 2.

At the same time, based on the consideration of the SoC estimator of each ESU in (1) and the calculation of the output power of the ESU in (7), it is obtained that

$$SoC_i = SoC_{i\,t=0} - \frac{1}{C_e V_{\text{in\_i}}} \int p_i \mathrm{d}t \tag{9}$$

By perturbing (9) and transferring the results into s domain, it is derived

$$s \cdot \hat{SoC}_i = -\hat{p}_i / (C_e V_{\text{in\_i}}) \tag{10}$$

Take the first-order low-pass filter into account,

$$\hat{p}_{\text{lpf\_i}} = G_{\text{lpf}} \cdot \hat{p}_i \tag{11}$$

where $G_{\text{lpf}}$ is shown as

$$G_{\text{lpf}} = \frac{\omega_c}{s + \omega_c} \tag{12}$$

where $\omega_c$ is the cutting frequency of the filter.

By combining (6), (10) and (11), it yields:

$$m_0 \hat{p}_{\text{lpf\_i}} = -n SoC_i^{n-1}(V_{dc}^* - V_{dc\_i}) \cdot \hat{p}_{\text{lpf\_i}} / (C_e V_{\text{in\_i}} \cdot sG_{\text{lpf}}) \quad (13)$$
$$- SoC_i^n \cdot \hat{v}_{dc\_i}$$

Then, (13) can be rewritten as

$$\hat{p}_{\text{lpf\_i}} = -\frac{SoC_i^n \cdot sG_{\text{lpf}}}{m_0 sG_{\text{lpf}} + k_{dc\_i}} \cdot \hat{v}_{dc\_i} \tag{14}$$

where

$$k_{dc\_i} = n SoC_i^{n-1}(V_{dc}^* - V_{dc\_i}) / (C_e V_{\text{in\_i}})$$

Meanwhile, at the point of common coupling (PCC), the power flow follows the relationship:

$$p_1 + p_2 = p_{\text{load}} \tag{15}$$

where $p_{\text{load}}$ is the load power at the PCC.

It can be assumed that the power cables in a dc system commonly do not present big voltage drops. This can be demonstrated by the line resistance of the power cable, as shown in Table II [21]. The line resistance of a dc system is determined by the cross-sectional area, materials and structure of the power cable. It is seen from Table II that the line resistance is commonly less than 0.04 Ω/km. Supposing that the active power of 2 kW flows through a resistive line of 1 km and the voltage rating of system is about 600V, it can be calculated that the voltage drop across the transmission line is less than 0.13 V. However, with the commonly used droop control, the voltage drop caused by the droop function is about 4 ~ 6 V, when the load is approximately 2 kW and the voltage level is around 600V. Compared to the voltage deviation caused by droop control, the voltage drop across the transmission line can be neglected. Hence,

$$v_{dc\_1} \approx v_{dc\_2} \approx v_{\text{dcload}} \tag{16}$$

where $v_{\text{dcload}}$ is the voltage at the PCC.

At the PCC, it is obtained that

$$p_{\text{load}} = \frac{v_{\text{dcload}}^2}{R_{\text{load}}} \tag{17}$$

where $R_{\text{load}}$ is the load resistance.

Thus, by substituting (17) into (15) and perturbing the obtained expression, with the consideration of (11), it yields

$$\hat{p}_{\text{lpf\_1}} + \hat{p}_{\text{lpf\_2}} = \frac{2V_{dc} \cdot G_{\text{lpf}}}{R_{\text{load}}} \hat{v}_{\text{dcload}} \tag{18}$$

By combining (14) and (18), the characteristic equation of the control system is reached as

$$A \cdot s^3 + B \cdot s^2 + C \cdot s + D = 0 \tag{19}$$

where $A$, $B$, $C$ and $D$ are

$$A = SoC_1^n R_{\text{load}}(m_0\omega_c + k_{dc\_2}) + SoC_2^n R_{\text{load}}(m_0\omega_c + k_{dc\_1})$$

$$B = SoC_1^n R_{\text{load}}(m_0\omega_c^2 + 2\omega_c k_{dc\_2}) + SoC_2^n R_{\text{load}}(m_0\omega_c^2 + 2\omega_c k_{dc\_1})$$
$$+ 2V_{\text{dcload}}(m_0\omega_c + k_{dc\_1})(m_0\omega_c + k_{dc\_2})$$

$$C = SoC_1^n R_{\text{load}} k_{dc\_2}\omega_c^2 + SoC_2^n R_{\text{load}} k_{dc\_1}\omega_c^2$$
$$+ 2V_{\text{dcload}}\omega_c(m_0\omega_c k_{dc\_1} + m_0\omega_c k_{dc\_2} + 2k_{dc\_1}k_{dc\_2})$$

$$D = 2V_{\text{dcload}} k_{dc\_1} k_{dc\_2}\omega_c^2$$

From (19), a stability analysis based on closed-loop poles can be done. By using the parameters shown in Table III, the dominant closed-loop poles with different SoCs and exponents are shown in Fig. 5. The dominant poles with different SoCs are shown with different styles of lines, while the poles with different exponents are shown with different numbers. It is found that in the given condition the closed-loop poles are all located on the left half of the plane, so the stability of the control system can be ensured.

### D. Power Sharing Speed Adjustment

As aforementioned, by using the SoC-based droop control method, the energy stored in the ESUs with higher SoC decreases faster than that in the ESUs with lower SoC. Thus, after a dynamic process, the SoC in each of the ESUs becomes equal and the output power of the distributed ESUs is equally shared.

The power sharing speed can be adjusted by changing the exponent n of SoC in (5). By combining (5) and (16),

TABLE II
Line Resistance for Conductors of Power Cables

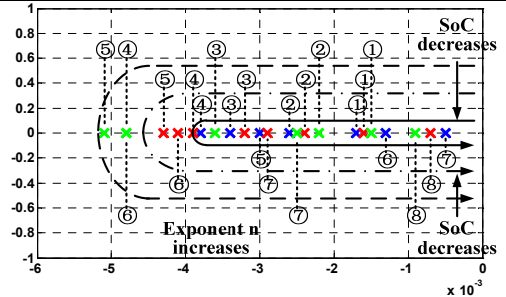| Cross-Sectional Area /mm² | Maximum Resistance of Conductor at 20°C | | |
| --- | --- | --- | --- |
| | Annealed Copper Conductor | | Aluminium or Aluminium Alloy Conductor Ωkm⁻¹ |
| | Plain Wires /Ωkm⁻¹ | Metal-coated Wires /Ωkm⁻¹ | |
| 800 | 0.0221 | 0.0224 | 0.0367 |
| 1600 | 0.0113 | 0.0113 | 0.0186 |
| 2000 | 0.0090 | 0.0090 | 0.0149 |



Fig. 5. Root locus plot of the SoC-based droop control with different SoCs and exponents.

$$\frac{p_{\text{lpf\_1}}}{SoC_1^n} = \frac{p_{\text{lpf\_2}}}{SoC_2^n} \qquad (20)$$

Because the changing of SoC is much slower than that of the output power, it can be assumed that

$$p_1 / p_2 \approx p_{\text{lpf\_1}} / p_{\text{lpf\_2}} = SoC_1^n / SoC_2^n \qquad (21)$$

Therefore, the load power can be shared according to $SoC^n$. Considering (9), (15) and (21), it yields

$$SoC_i = SoC_{i\,t=0} - \frac{p_{\text{load}}}{C_e V_{\text{in\_i}}} \int \frac{SoC_i^n}{\sum SoC_i^n} dt \qquad (22)$$

The numeric solutions of (22) can be achieved and the results are shown in Fig. 6. It is seen that with larger exponent n, $SoC_1$ and $SoC_2$ become equal in a shorter time. At $t = 1500$ s, the differences between $SoC_1$ and $SoC_2$ are 3.24%, 1.86% and 0.34% when the exponent n is selected as 2, 3 and 6, respectively. Meanwhile, the power sharing speed becomes faster as n increases. At $t = 1500$ s, the differences between $p_1$ and $p_2$ are 118.2 W, 100.3 W and 36.5 W when the exponent n is selected as 2, 3 and 6, respectively.

*E. Limitation of the Exponent of SoC*

As demonstrated before, the power sharing speed can be regulated by the exponent n of each SoC. In order to learn the upper limit of the exponent, the derivation is obtained as follows.

The initial sharing of the load power is changed by different exponent n. From (15) and (21), the initial output power of each converter can be derived as

$$p_{i\,t=0} = \frac{SoC_{i\,t=0}^n}{\sum SoC_{i\,t=0}^n} \cdot p_{\text{load}} \qquad (23)$$

Due to the limitation of the maximum output power of each interface converter, it is achieved

$$\frac{SoC_{i\,t=0}^n}{\sum SoC_{i\,t=0}^n} \le \frac{p_{i\,\text{max}}}{p_{\text{load}}} \qquad (24)$$

Inequality (24) shows the first limitation of the exponent n. If n is larger than its upper limit, the initial output power of the interface converter will exceed its maximum power rating. The relationship between the initial output power and the exponent n is shown in Fig. 7, where the output power of each converter should not reach the unsafe region.

Meanwhile, except for the consideration of the maximum power rating of the converter, the maximum dc voltage deviation involved by droop control should be taken into account as another restriction for the upper limit of the exponent n. Take Converter #1 as an example. It can be derived from (5) that the deviation of DC bus voltage is shown as

$$\Delta v_{\text{dc1}} = \frac{m_0}{SoC_1^n} \cdot p_{\text{lpf1}} \qquad (25)$$

where the DC voltage deviation $\Delta v_{\text{dc1}}$ should not exceed its maximum acceptable value

Considering the proportional load power sharing in (21) and the relationship in (15) and (17), it yields

$$\Delta v_{\text{dc1}} = \frac{m_0}{SoC_1^n + SoC_2^n} \cdot \frac{(v_{\text{dc}}^* - \Delta v_{\text{dc1}})^2}{R_{\text{load}}} \qquad (26)$$

TABLE III
System Parameters

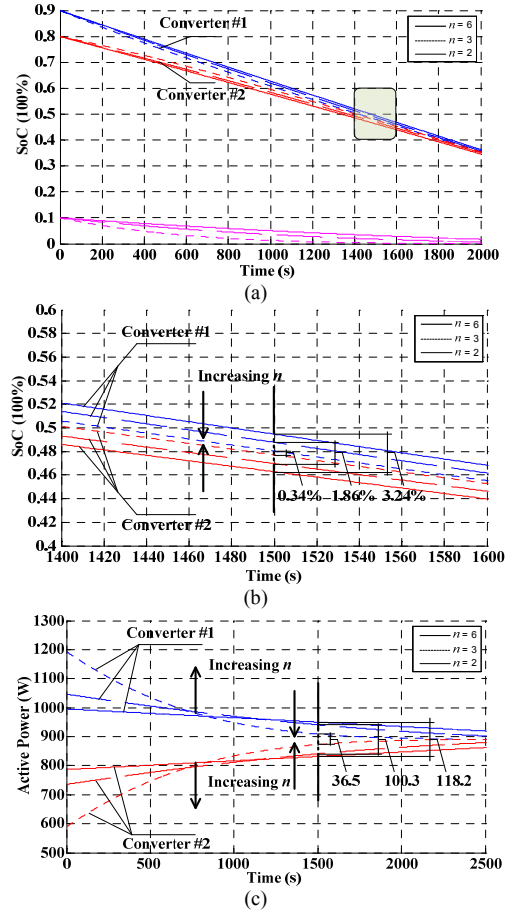| Item | Symbol | Value | Unit |
|---|---|---|---|
| Initial $SoC_1$ | $SoC_{1\,t=0}$ | 90 | % |
| Initial $SoC_2$ | $SoC_{2\,t=0}$ | 80 | % |
| LPF Cutting Frequency | $\omega_c$ | 126 | rads⁻¹ |
| Converter #1 Input Voltage | $V_{\text{in\_1}}$ | 200 | V |
| Converter #2 Input Voltage | $V_{\text{in\_2}}$ | 200 | V |
| Load Resistance | $R_{\text{load}}$ | 200 | Ω |
| Load Power | $p_{\text{load}}$ | 1800 | W |
| Power Rating of the Converter | $p_{\text{max}}$ | 2500 | W |



Fig. 6. Speed regulation of power sharing with different exponent n. (a) The results of the SoC. (b) Detail of the square region in the waveforms of SoCs. (c) The results of the output power.
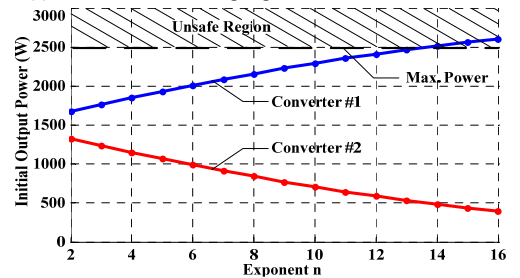


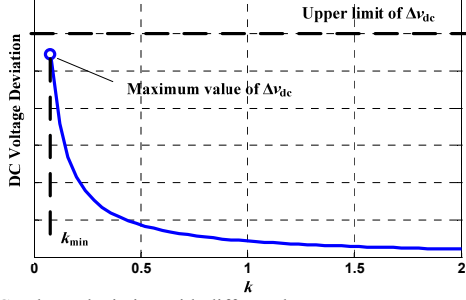Fig. 7. Initial output power of each converter with different exponent n.

Fig. 8. DC voltage deviation with different k.

The deviation of DC voltage $\Delta v_{dc1}$ can be reached by solving the quadratic equation (26), as shown as

$$\Delta v_{dc1} = v_{dc}^* + \frac{(SoC_1^n + SoC_2^n)R_{load} - \sqrt{\Delta}}{2m_0} \quad (27)$$

$$\Delta = 4m_0 v_{dc}^* R_{load}(SoC_1^n + SoC_2^n) + R_{load}^2(SoC_1^n + SoC_2^n)^2$$

where the other solution of (26) is rejected since $\Delta v_{dc1}$ should be less than $v_{dc}^*$.

Assuming that

$$k = SoC_1^n + SoC_2^n \quad (28)$$

Therefore, (27) can be rewritten as

$$\Delta v_{dc1} = v_{dc}^* + \frac{kR_{load} - \sqrt{4m_0 v_{dc}^* R_{load}k + R_{load}^2 k^2}}{2m_0} \quad (29)$$

For $\forall k > 0$, it can be obtained that

$$\frac{d\Delta v_{dc1}}{dk} = \frac{R_{load}}{2m_0}(1 - \frac{2m_0 v_{dc}^* + R_{load}k}{\sqrt{4m_0 v_{dc}^* R_{load}k + R_{load}^2 k^2}}) < 0 \quad (30)$$

As a result, (29) is a decreasing function of $k$.

Meanwhile, for $\forall k$, $\Delta v_{dc1}$ should be less than its maximum value, so

$$[\Delta v_{dc1}(k)]_{max} \leq \Delta v_{dc\,max} \quad (31)$$

Notice that

$$k = SoC_1^n + SoC_2^n \geq (SoC_{1\,min})^n + (SoC_{2\,min})^n = k_{min} \quad (32)$$

It yields

$$[\Delta v_{dc1}(k)]_{max} = \Delta v_{dc1}(k_{min}) \leq \Delta v_{dc\,max} \quad (33)$$

The curve of DC deviation versus $k$ is shown in Fig. 8. It is seen that the maximum value of DC deviation is achieved when $k$ has the minimum value and the maximum deviation should be lower than its upper limit. Since $0 < SoC_{i\,min} \leq 1$ ($i = 1, 2$), it is achieved from (32) that with larger exponent n, $k_{min}$ is smaller, which means that $[\Delta v_{dc1}(k)]_{max}$ is larger. Therefore, it can be concluded that the upper limit of the exponent n should be determined in order to guarantee that $[\Delta v_{dc1}(k)]_{max}$ is lower than its maximum acceptable value.

The lower limit of n is determined by minimizing the power sharing error within the acceptable range in the preset time duration. From (22), by taking the derivative of $SoC_1$ and $SoC_2$ for the condition of i = 1 and 2, it can be obtained that

$$\frac{dSoC_1}{SoC_1^n} = \frac{dSoC_2}{SoC_2^n} \quad (34)$$

In order to enhance the SoC balance speed, n is selected larger than 1 here. Thus, by solving the differential equation (34),

$$\frac{1}{1-n}(SoC_1^{1-n} - SoC_2^{1-n}) = \frac{1}{1-n}(SoC_{1\,t=0}^{1-n} - SoC_{2\,t=0}^{1-n}) \quad (35)$$

Then, it yields that

$$(\frac{SoC_1}{SoC_2})^{1-n} = 1 + \frac{SoC_{1\,t=0}^{1-n} - SoC_{2\,t=0}^{1-n}}{SoC_2^{1-n}} \quad (36)$$

When $SoC_{1\,t=0} \geq SoC_{2\,t=0}$, it is derived that $(SoC_1/ SoC_2)|_{t=T} \leq 1 + \varepsilon$. Here, $\varepsilon$ is the variable presenting the SoC balancing accuracy and $T$ is the preset time duration. The acceptable accuracy should be achieved within the time duration $T$. It should be noticed that $(SoC_1/ SoC_2)|_{t=T} \geq 1$ and $1 - n < 0$. Therefore, by using (36), it can be concluded that

$$1 + \frac{SoC_{1\,t=0}^{1-n} - SoC_{2\,t=0}^{1-n}}{(SoC_2|_{t=T})^{1-n}} \geq (1+\varepsilon)^{1-n} \quad (37)$$

By solving the transcendental equation (37), the minimum value of n can be determined.

When $SoC_{1\,t=0} < SoC_{2\,t=0}$, it is derived that $(SoC_1/ SoC_2)|_{t=T} \geq 1 - \varepsilon$. It should be also noticed that $(SoC_1/ SoC_2)|_{t=T} < 1$ and $1 - n < 0$. Therefore, also by using (36), it yields

$$1 + \frac{SoC_{1\,t=0}^{1-n} - SoC_{2\,t=0}^{1-n}}{(SoC_2|_{t=T})^{1-n}} \leq (1-\varepsilon)^{1-n} \quad (38)$$

By solving the transcendental equation (38), the minimum value of n can be determined.

A case study is provided here as an example of determining the limitation of the exponent n. If setting $T = 1500$ s, $\varepsilon = 1\%$, the numeric solution of the above equations can be obtained and the lower limit of n is derived as 6. Considering the power rating of each converter, the upper limit of n is determined as 14 and considering the maximum deviation of DC voltage, the upper limit of n is 8. As a result, the exponent n should be selected within the range of $6 \leq n \leq 8$.

For the above SoC-based adaptive droop control method, it should be noticed that the SoC of each ESU cannot be lower than its minimum value. When the SoC of ESU reaches its minimum value $SoC_{min}$, the ESU should be cut off and wait for the next charging process.

## III. SIMULATION STUDY

Simulations based on Matlab/Simulink are performed to evaluate the performance of the SoC-based droop control method. The parameters of the system are listed in Table III. Here, the ESU model employed is shown in Section II (B).

*Case I: Performance of the Proposed Method with Different Exponents*

When the exponent n equals to 2, the waveforms of SoC and output power in each converter are shown in Fig. 9 (a) and (b), respectively. The initial values of $SoC_1$ and $SoC_2$ are 90% and 80%, respectively. During the operation, ESU #1 with larger SoC delivers more power than ESU #2 with lower SoC. As a result, $SoC_1$ and $SoC_2$ trend to balance, thus equalizing the output power of each converter. Similar results are obtained when n equals to 6, as shown in Fig. 10.

The same length of time duration is selected when capturing the figures. When n = 2, the difference between $SoC_1$ and $SoC_2$ changes from 10% to 1.9% and the difference between $p_1$ and $p_2$ changes from 214.3 W to 50.9 W. When n = 6, the difference between $SoC_1$ and $SoC_2$ changes from 10% to almost 0 and the difference between $p_1$ and $p_2$ changes from 612.0 W to almost 0. By comparing Fig. 9 and Fig. 10, it can be found that with larger exponent n, the faster dynamic process of power sharing equalization is achieved. This is in accordance with the theoretical analysis.

*Case II: Performance of the Proposed Method with Various Initial SoC Differences*

In the above test in Case I, the difference between the initial SoCs is set to 10%. In order to test the performance of the proposed method, the scenarios with other initial differences are tested. Here, the initial SoC of ESU #1 is fixed to 90%, while the initial SoC of ESU #2 varies from 40% to 80%. With the proposed SoC-based droop control method, the waveforms of $SoC_1 - SoC_2$ and $p_1 - p_2$ are shown in Fig. 11. It is seen that the differences of SoC and output power gradually become zero. Hence, with various initial differences the proposed method is still valid.

*Case III: Performance of the Proposed Method with the Consideration of the Error in the SoC Estimation*

The influence of the ampere-hour perturbation is tested by considering the error in the estimated SoC. As shown in Fig. 12, when the random error is involved, the ratio of $(SoC_1/SoC_2)^n$ is influenced. However, the ratio of SoC still gradually becomes 1 and the output power equalization is also achieved, so the viability of the proposed method can be shown.

*Case IV: Performance of the Proposed Method with Load Peaks*

The dynamic performance of the SoC-based droop control method with 60 s and 30 s load peaks are shown in Fig. 13. Take the results of 60 s load peak as an example. At the beginning of the power sharing process, the initial difference of the SoC is 10%. Then, at $t$ = 40 s, the difference reduces to 4.45% with the proposed method. At that moment, the load peak occurs and the SoC decreases with a larger slope. At $t$ = 100 s, the SoC reduces to 0.47%. From that moment, the load peak ends and in the following process, the SoC decreases with a smaller slope and the gradually becomes equal. The corresponding process is shown in the waveform of the output power. The difference of the output power changes as follows: 199.5 W – 118.5 W – 25.4 W – 5.7 W.

*Case V: Performance of the Proposed Method with Bus Failures*

The ride-through capability of the proposed method is tested by considering the bus failure. As shown in Fig. 14, a

DESS with three ESUs is taken into account. At $t$ = 20 s and 60 s, the local bus #3 and #2 are cut off in sequence due to the bus failures. It is seen that at any time the load power can be properly shared among the remaining active ESUs by using SoC-based droop control method.
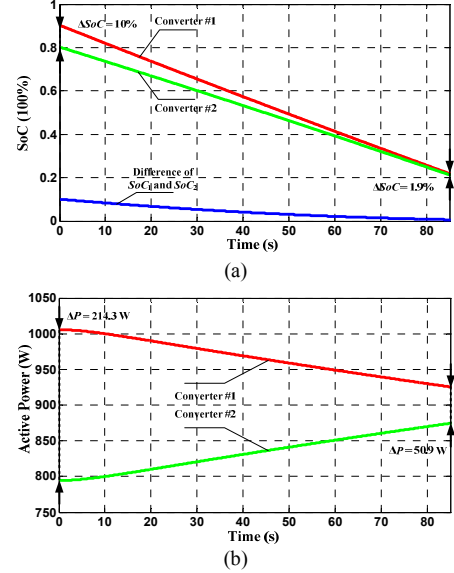


Fig. 9. SoC and power sharing waveforms for the SoC-based droop control when n = 2.
(a) Waveforms of $SoC_1$ and $SoC_2$. (b) Waveforms of output power of each converter.
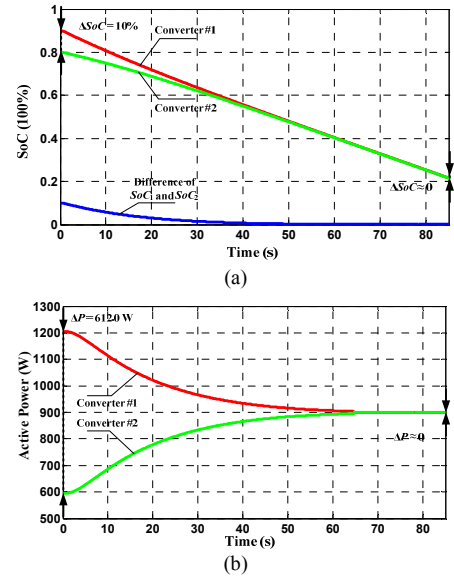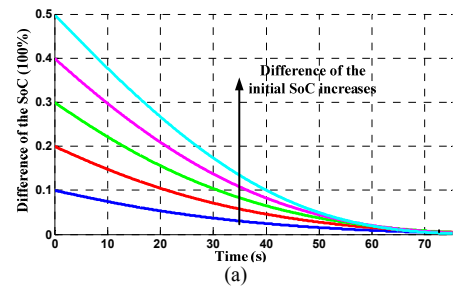


Fig. 10. SoC and power sharing waveforms for the SoC-based droop control when n = 6.
(a) Waveforms of $SoC_1$ and $SoC_2$. (b) Waveforms of output power of each converter.
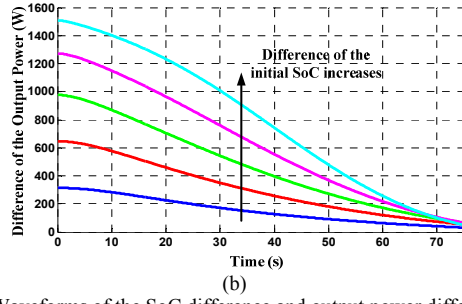
Fig. 11. Waveforms of the SoC difference and output power difference.
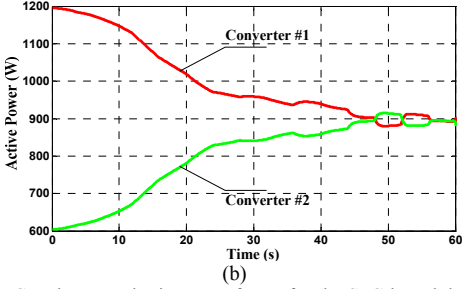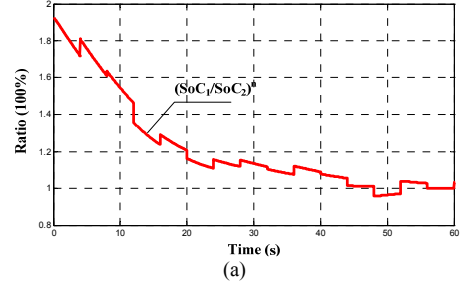(a) Waveforms of $SoC_1$ - $SoC_2$. (b) Waveforms of $p_1$ - $p_2$.



Fig. 12. SoC and power sharing waveforms for the SoC-based droop control considering the random error in the estimated SoC.
(a) Waveforms of $(SoC_1/SoC_2)^n$. (b) Waveforms of output power of each converter.
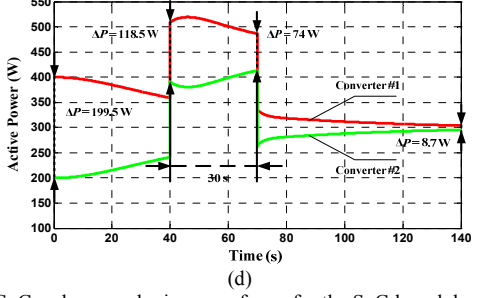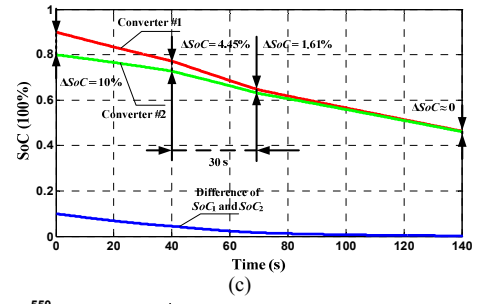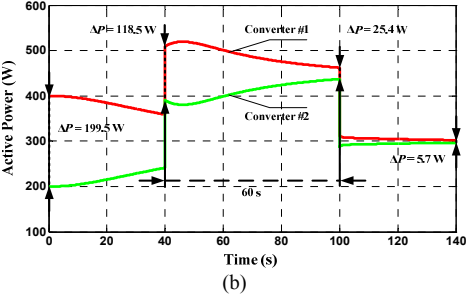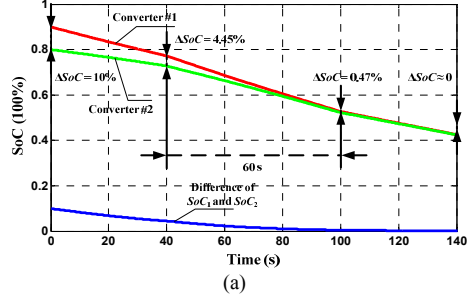


Fig. 13. SoC and power sharing waveforms for the SoC-based droop control with load peaks.
(a) Waveforms of $SoC_1$ and $SoC_2$ with 60 s load peaks.
(b) Waveforms of output power of each converter with 60 s load peaks.
(c) Waveforms of $SoC_1$ and $SoC_2$ with 30 s load peaks.
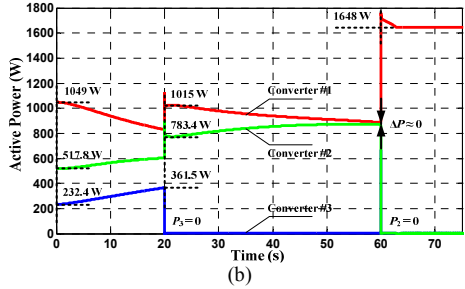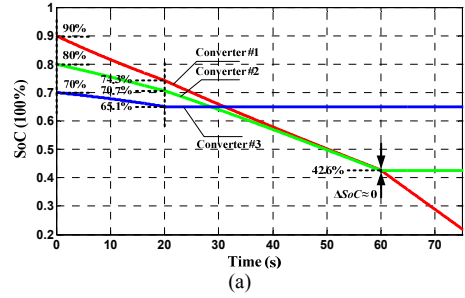(d) Waveforms of output power of each converter with 30 s load peaks.



Fig. 14. SoC and power sharing waveforms for the SoC-based droop control considering bus failures
(a) Waveforms of SoC of each converter. (b) Waveforms of output power of each converter.

## IV. EXPERIMENTAL VALIDATION

In this paper, the SoC balancing is achieved by using improved droop control method. Therefore, the paper aims at the power sharing between the droop-controlled PCSs. The H-bridge boost converter with PWM method is employed in this paper and the experimental setup is composed of two parallel converters. Meanwhile, limited to the existing test-bed condition, the ESU is modeled by using real-time simulation. More particularly, the prototype consists of two parts. One part is the 2×2.2 kW parallel

converters (real hardware) and the other part is the models of the ESUs as shown in Section II (B) (real-time simulation in dSPACE 1103). The input power for each converter is measured in the real hardware converter system and transferred to the real-time model of the ESU. Then, the key variables, like SoC, are estimated in the real-time model and transferred to the control diagram for calculating the droop coefficients. The configuration of the experimental setup is shown in Fig. 15 and the photo of the prototype is shown in Fig. 16. In order to evaluate the efficiency of the basic interfacing circuit of H-bridge boost converter, the commonly used loss modeling method is employed [22] and the converter efficiency is shown in Fig. 17.

Similar as that in the simulations, the SoCs and the output power waveforms are shown for n = 2, 3 and 6, as shown in Fig. 18, Fig. 19 and Fig. 20. The same length of time duration is selected when capturing the figures. When n = 2, the difference between $SoC_1$ and $SoC_2$ changes from 10% to 1.4% and the difference between $p_1$ and $p_2$ changes from 216.7 W to 45.0 W. When n = 3, the difference between $SoC_1$ and $SoC_2$ changes from 10% to 0.95% and the difference between $p_1$ and $p_2$ changes from 311.7 W to 16.7 W. When n = 6, the difference between $SoC_1$ and $SoC_2$ changes from 10% to almost 0 and the difference between $p_1$ and $p_2$ changes from 610.0 W to almost 0. Here, when n = 6, the accurate power sharing can be reached within the time duration, and the initial output power of each converter is guaranteed to be lower than the maximum power rating.

It is seen from the experimental results that:

1) With the proposed method, the SoCs in different ESUs are gradually balanced. Meanwhile, the output power is equalized.

2) Comparing the results in Fig. 18, Fig. 19 and Fig. 20, with high exponent n, the SoC balancing and load power equalization speed is higher.

## V. CONCLUSION

In order to reach dynamic SoC balancing and power sharing of distributed energy storage systems in DC micro-grids, an SoC-based adaptive droop control method is proposed in this paper. Particularly, the droop coefficient is inversely proportional to the $n^{th}$ order of SoC. By using this control method, the ESU with higher SoC delivers more power, while the one with lower SoC delivers less power. The difference between the SoCs becomes smaller, and the output power of the converters gradually becomes equal. Meanwhile, the power sharing speed is adjusted by changing the exponent n of SoC. The small signal model of the control system is derived and the system stability is guaranteed by the root locus analysis. The limit of the exponent is determined with respect to the power rating of each converter, the maximum value of DC voltage deviation and the load power sharing accuracy. The proposed approach is used for balancing the SoCs of distributed ESUs and the operation does not require communications among the units. Hence, the method is suitable for the micro-grid applications.

Furthermore, the proposed method in this paper can be extended to AC micro-grids with inductive line impedances. The SoC-based approach can be employed in the $P - f$ droop control in order to reach a proper active power sharing.
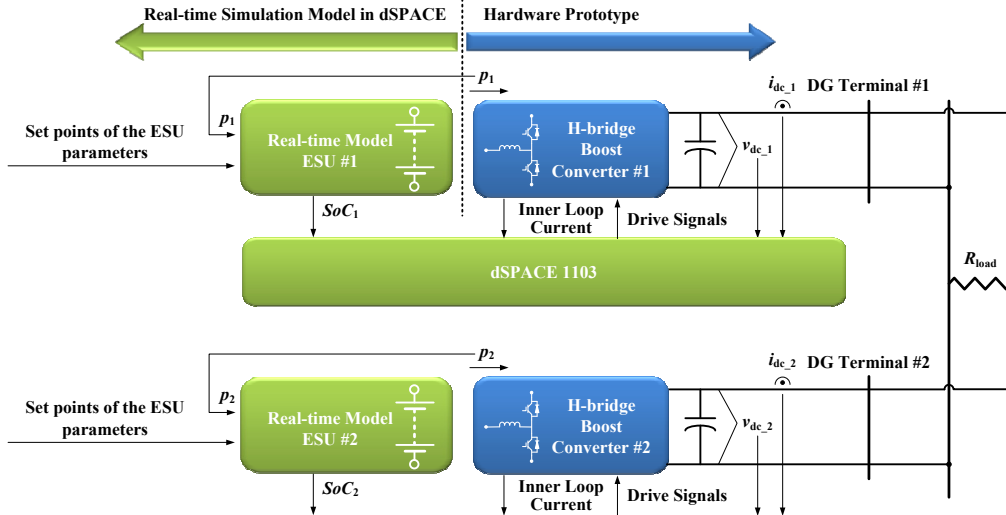


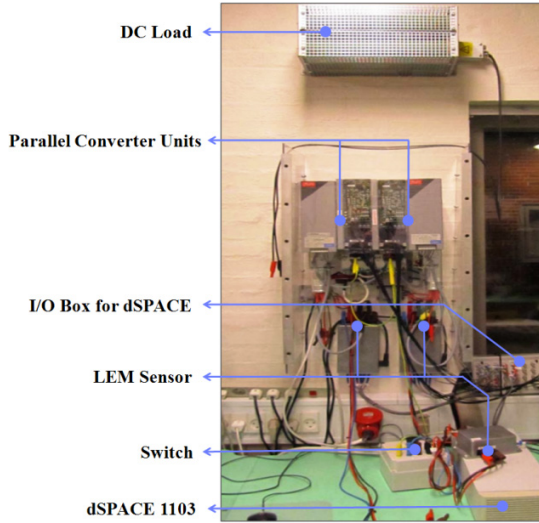Fig. 15. Configuration of the experimental setup.
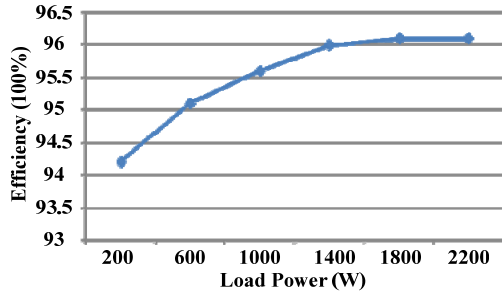
Fig. 16. Photo of the prototype.



Fig. 17. Efficiency evaluation of the commonly used interfacing circuit – H-bridge boost converter.



Fig. 18. SoC and power sharing waveforms by the SoC-based droop control when n = 2.
(a) Waveforms of $SoC_1$ and $SoC_2$. (b) Waveforms of output power of each converter.



Fig. 19. SoC and power sharing waveforms by the SoC-based droop control when n = 3.
(a) Waveforms of $SoC_1$ and $SoC_2$. (b) Waveforms of output power of each converter.
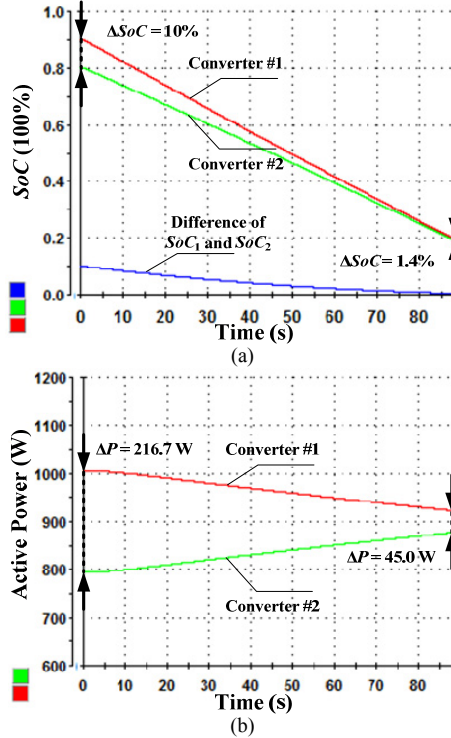


Fig. 20. SoC and power sharing waveforms by the SoC-based droop control when n = 6.
(a) Waveforms of $SoC_1$ and $SoC_2$. (b) Waveforms of output power of each converter.
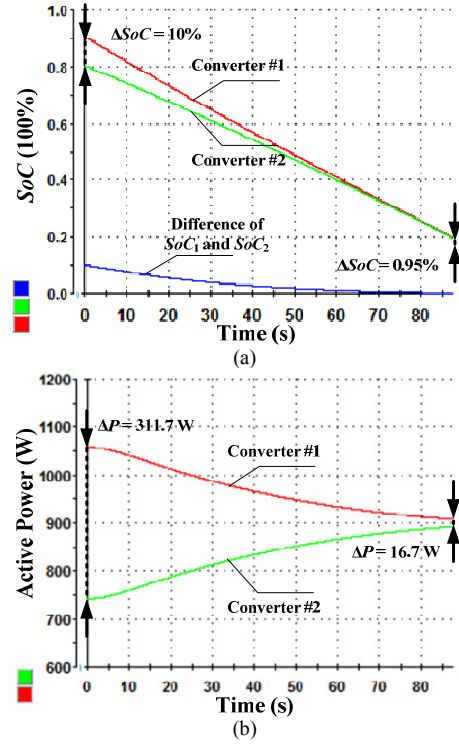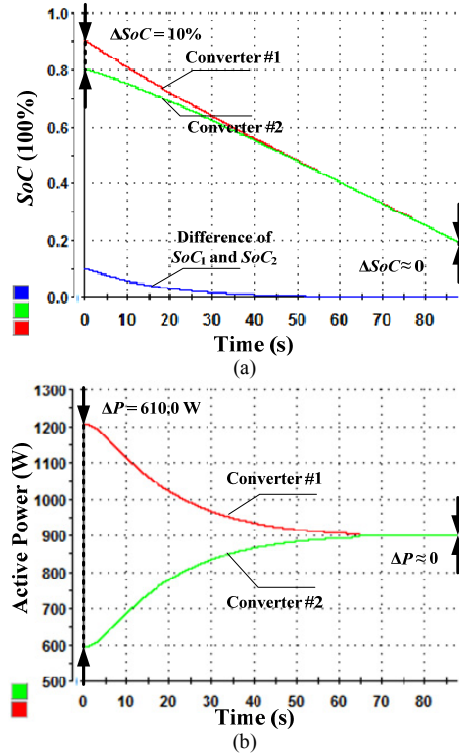
# REFERENCES

[1] R. Lasseter, A. Akhil, C. Marnay, J. Stevens, et al, "The certs microgrid concept - white paper on integration of distributed energy resources," Technical Report, U.S. Department of Energy, 2002.

[2] A. Pratt, P. Kumar and T. V. Aldridge, "Evaluation of 400V DC distribution in telco and data centers to improve energy efficiency," in Proc. of INTELEC, pp. 32-39, 2007.

[3] H. Kakigano, M. Nomura and T. Ise, "Loss evaluation of dc distribution for residential houses compared with ac system," in Proc. of IPEC, pp. 480-486, 2010.

[4] H. Valderrama-Blavi, J. M. Bosque, F. Guinjoan, L. Marroyo and L. Martínez-Salamero, "Power adaptor device for domestic dc microgrids based on commercial MPPT inverter," IEEE Trans. Ind. Electron., vol. 60, no. 3, pp. 1191-1203, 2013.

[5] X. Lu, J. M. Guerrero, K. Sun and J. C. Vasquez, "An improved control method for DC microgrids based on low bandwidth communication with DC bus voltage restoration and enhanced current sharing accuracy," IEEE Trans. Power Electron., 2013. [Online]. Available: http://dx.doi.org/10.1109/TPEL.2013.2266419.

[6] J. M. Guerrero, J. C. Vasquez, J. Matas, G. G. De Vicuña and M. Castilla, "Hierarchical control of droop-controlled AC and DC microgrids - a general approach toward standardization," IEEE Trans. Ind. Electron., vol. 58, no. 1, pp. 158-172, 2011.

[7] K. Sun, L. Zhang, Y. Xing and J. M. Guerrero, "A distributed control strategy based on DC bus signaling for modular photovoltaic generation systems with battery energy storage," IEEE Trans. Power Electron., vol. 26, no. 10, pp. 3032-3045, 2011.

[8] M. Sechilariu, B. Wang and F. Locment, "Building integrated photovoltaic system with energy storage and smart grid communication," IEEE Trans. Ind. Electron., vol. 60, no. 4, pp. 1607-1618, 2013.

[9] X. Lu, J. M. Guerrero, K. Sun, J. C. Vasquez, R. Teodorescu, et al, "Hierarchical control of parallel AC-DC converter interfaces for hybrid microgrids," IEEE Trans. Smart Grid, 2013. [Online]. Available: http://dx.doi.org/10.1109/TSG.2013.2272327.

[10] D. Dong, I. Cvetkovic, D. Boroyevich, W. Zhang, R. Wang, et al, "Grid-interface bi-directional converter for residential DC distribution systems – part one: high-density two-stage topology," IEEE Trans. Power Electron., vol. 28, no. 4, pp. 1655-1666, 2013.

[11] H. Kakigano, Y. Miura and T. Ise, "Distribution voltage control for dc microgrids using fuzzy control and gain-scheduling technique," IEEE Trans. Power Electron., vol. 28, no. 5, pp. 2246-2258, 2013.

[12] J. M. Guerrero, P. C. Loh, T.-L. Lee and M. Chandorkar, "Advanced control architectures for intelligent microgrids – part II: power quality, energy storage, and ac/dc microgrids," IEEE Trans. Ind. Electron., vol. 60, no. 4, pp. 1263-1270, 2013.

[13] H. –S. Park, C. –E. Kim, C. –H. Kim, G. –W. Moon and J. –H. Lee, "A modularized charge equalizer for an HEV Lithium-Ion battery string," IEEE Trans. Ind. Electron., vol. 56, no. 5, pp. 1464-1476, 2009.

[14] A. Manenti, A. Abba, A. Merati, S. M. Savaresi and A. Geraci, "A new BMS architecture based on cell redundancy," IEEE Trans. Ind. Electron., vol. 58, no. 9, pp. 4314-4322, 2011.

[15] J. Kim, J. Shin, C. Chun and B. H. Cho, "Stable configuration of a Li-Ion series battery pack based on a screening process for improved voltage/SoC balancing," IEEE Trans. Power Electron., vol. 27, no. 1, pp. 411-424, 2012.

[16] L. M. Tolbert, F. Z. Peng, T. Cunnyngham and J. N. Chiasson, "Charge balance control schemes for cascade multilevel converter in hybrid electric vehicles," IEEE Trans. Ind. Electron., vol. 49, no. 5, pp. 1058-1064, 2002.

[17] L. Maharjan, S. Inoue, H. Akagi and J. Asakura, "State-of-charge (SOC) - balancing control of a battery energy storage system based on a cascade PWM converter," IEEE Trans. Power Electron., vol. 24, no. 6, pp. 1628-1636, 2009.

[18] H. Zhou, T. Bhattacharya, T. Duong, T. S. T. Siew and A. M. Khambadkone, "Composite energy storage system involving battery and ultracapacitor with dynamic energy management in microgrid applications," IEEE Trans. Power Electron., vol. 26, no. 3, pp. 923-930, 2011.

[19] V. H. Johnson, A. A. Pesaran and T. Sack, "Temperature-dependent battery models for high-power Lithium-Ion batteries," in Proc. of 17th Annual Electric Vehicle Symposium, Montreal, Canada, Oct 15-18, 2000.

[20] D. D. González and R. Diosi. "Accelerated life testing and life-time prediction of Lithium Ion batteries connected to wind turbine," Master Thesis, Dept. Energy Technology, Aalborg University, 2011.

[21] International standard for conductors of insulated cables, IEC-60228, 2004.

[22] D. Xu, H. Lu, L. Huang, S. Azuma, M. Kimata, et al, "Power loss and junction temperature analysis of power semiconductor devices," IEEE Trans. Ind. Appl., vol. 38, no. 5, pp. 1426-1431, 2002.
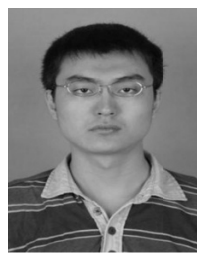
**Xiaonan Lu** (S'11) was born in Tianjin, China, 1985. He received the B. E. and Ph. D. degree in electrical engineering from Tsinghua University, Beijing, China, in 2008 and 2013, respectively. From Sep. 2010 to Aug. 2011 he was a guest Ph. D. student at Department of Energy Technology, Aalborg University, Denmark.

His research interests are control of power electronics interfacing converters for renewable generation systems and microgrids, multilevel converters, and matrix converters.

**Kai Sun** (M'12) was born in Beijing, China, 1977. He received the B.E., M.E., and Ph.D. degrees in electrical engineering all from Tsinghua University, Beijing, China, in 2000, 2002, and 2006, respectively. In 2006, he joined the faculty of Tsinghua University as a Lecturer of Electrical Engineering, where he is currently an Associate Professor. From Sep. 2009 to Aug. 2010 he was a Visiting Scholar at Department of Energy Technology, Aalborg University, Denmark.

He has authored more than 80 technical papers, including 9 international journal papers. His main research interests are power converters for renewable generation systems and AC motor drives. Dr. Sun received the Delta Young Scholar Award in 2013.

**Josep M. Guerrero** (S'01-M'04-SM'08) received the B.S. degree in telecommunications engineering, the M.S. degree in electronics engineering, and the Ph.D. degree in power electronics from the Technical University of Catalonia, Barcelona, in 1997, 2000 and 2003, respectively. He was an Associate Professor with the Department of Automatic Control Systems and Computer Engineering, Technical University of Catalonia, teaching courses on digital signal processing, field-programmable gate arrays, microprocessors, and control of renewable energy. In 2004, he was responsible for the Renewable Energy Laboratory, Escola Industrial de Barcelona. Since 2011, he has been a Full Professor with the Department of Energy Technology, Aalborg University, Aalborg East, Denmark, where he is responsible for the microgrid research program. From 2012 he is also a guest Professor at the Chinese Academy of Science and the Nanjing University of Aeronautics and Astronautics. His research interests is oriented to different microgrid aspects, including power electronics, distributed energy-storage systems, hierarchical and cooperative control, energy management systems, and optimization of microgrids and islanded minigrids. Prof. Guerrero is an Associate Editor for the IEEE TRANSACTIONS ON POWER ELECTRONICS, the IEEE TRANSACTIONS ON INDUSTRIAL ELECTRONICS, and the IEEE Industrial Electronics Magazine, and an Editor for the IEEE TRANSACTIONS on SMART GRID. He has been Guest Editor of the IEEE TRANSACTIONS ON POWER ELECTRONICS Special Issues: Power Electronics for Wind Energy Conversion and Power Electronics for Microgrids; the IEEE TRANSACTIONS ON INDUSTRIAL ELECTRONICS Special Sections: Uninterruptible Power Supplies systems, Renewable Energy Systems, Distributed Generation and Microgrids, and Industrial Applications and Implementation Issues of the Kalman Filter; and the IEEE TRANSACTIONS on SMART GRID Special Issue on Smart DC Distribution Systems. He was the chair of the Renewable Energy Systems Technical Committee of the IEEE Industrial Electronics Society.

**Juan C. Vasquez** (M'12) received the B.S. degree in Electronics Engineering from Autonoma University of Manizales, Colombia in 2004 where he has been teaching courses on digital circuits, servo systems and flexible manufacturing systems. In 2009, He received his Ph.D. degree from the Technical University of Catalonia, Barcelona, Spain in 2009 at the Department of Automatic Control Systems and Computer Engineering, from Technical University of Catalonia, Barcelona (Spain), where he worked as Post-doc Assistant and also teaching courses based on renewable energy systems. Currently, he is an Assistant Professor at Aalborg University in Denmark. His research interests include modeling, simulation, networked control systems and optimization for power management systems applied to Distributed Generation in AC/DC Microgrids.

**Lipei Huang** was born in Jiangsu, China, 1946. He received the B.E. and M.E. degrees in electrical engineering from Tsinghua University, Beijing, China, in 1970 and 1982, respectively, and the Ph.D. degree from Meiji University, Tokyo, Japan, in 1996. In 1970, he joined the Department of Electrical Engineering, Tsinghua University. Since 1994, he has been a Professor in the Department of Electrical Engineering, Tsinghua University. In 1987, he was a Visiting Scholar of Electrical Engineering at the Tokyo Institute of Technology, for three months, and at Meiji University, Kawasaki, Japan, for nine months. He joined the research projects of K. Matsuse Laboratory, Department of Electrical Engineering, Meiji University, Kawasaki, Japan, as a Visiting Professor in 1993.
He has authored more than 100 technical papers and holds 7 patents. His research interests are in power electronics and adjustable-speed drives.
Prof. Huang received the Education Awards from the China Education Commission and Beijing People's Government in 1997. From 2001 to 2003 he was a Delta Scholar.